Physical Interactions Between Millimeter Waves and Human Body: From Macro- to Micro-Scale

Giulia Sacco, Maxim Zhadobov

IEEE Journal of Microwaves

Received 6 March 2024; revised 8 May 2024; accepted 24 May 2024. Date of publication 21 June 2024; date of current version 12 July 2024.

Digital Object Identifier 10.1109/JMW.2024.3407712

Physical Interactions Between Millimeter Waves and Human Body: From Macro- to Micro-Scale

GIULIA SACCO (Member, IEEE) AND MAXIM ZHADOBOV (Senior Member, IEEE)

(Regular Paper)

Univ Rennes, CNRS, CentraleSupelec, Nantes Université, IETR UMR 6164, F 35000 Rennes, France

CORRESPONDING AUTHOR: Giulia Sacco (e-mail: giulia.sacco@cnrs.fr).

This project has received funding from the European Union's Horizon Europe research and innovation program under Grant Agreement N°101063966 (Marie Skłodowska-Curie IN-SIGHT Project); in part by Labex CominLabs (ANR-10-LABX-07-01) through EM-ART Project; and in part by PNREST ANSES, ANSES-23-RF-03 through EXPO-5G Project, ANSES-23-RF-07 through CHILD_5G Project.

ABSTRACT With the massive deployment of 5G worldwide the entire population is expected to be exposed to millimeter waves (mmWs), representing new frequencies recently introduced into our environmental electromagnetic (EM) background. From this perspective, the interactions between mmWs and human tissues have been actively investigated during the past few years at various levels. This article reviews recent publications in this field, from macro- to micro-scale. The role of different parameters is considered, including the characteristics of the impinging field (angle of incidence, polarization, and source type), age, presence of clothing, curvature of the body surface, and inter-individual differences. Finally, findings on recent microdosimetry studies at mmWs are summarized highlighting the impact of micro-scale heterogeneity related to the presence of skin sub-structures and organelles inside the cells on the local power distribution and heating.

INDEX TERMS 5G, millimeter wave (mmW), macro-scale, micro-scale, electromagnetic dosimetry.

I. INTRODUCTION

With the ongoing massive deployment of 5G, new frequency bands have been introduced for wireless networking. According to the International Telecommunication Union (ITU), the mobile data traffic is expected to reach 5 zettabyte/month by 2030 [1] and the number of devices connected to internet will exceed 75.4 billion by 2025 [2]. To address the increasing demand in data traffic, robust high data-rate transmissions and new services, frequencies in the 24–28 GHz range are under testing or deployment, depending on the country, and some countries are also considering the 60 GHz band [3], [4], [5], [6], [7], [8]. Furthermore, mobile devices operating in the 37–40 GHz range are already available on the market [9].

Upcoming mass development of millimeter wave (mmW) technologies will induce the exposure of the users to frequencies to which humans have never been exposed so far. At mmWs, the power transmission coefficient at the air/skin interface is higher than at centimeter and decimeter waves (55% at 30 GHz and 63% at 60 GHz). The shallow penetration depth, essentially limited to cutaneous layers, results in locally high exposure levels in the near-surface tissues compared to lower microwave frequencies, even for relatively low levels of the incident power density.

The state of knowledge related to various aspects of interactions between the human body and mmWs was reported in [10], [11], [12], [13], where the attention was essentially focused on permittivity measurements, body-centric communications, exposure assessment in canonical scenarios, as well as on thermal modelling. The main goal of this review paper is to provide an overview of recent publications in the field of mmW interactions with the human body. The fundamental physical aspects of the mmW/body interactions, followed by the summary of the mmW dosimetric quantities, are described in the Section II. Section III reports the advancements in mmW tissue-equivalent models and phantoms. Recent results related to the mmW power deposition in the near-surface tissues are summarized in Section IV, where the impact of various exposure parameters and conditions (age, clothing, body

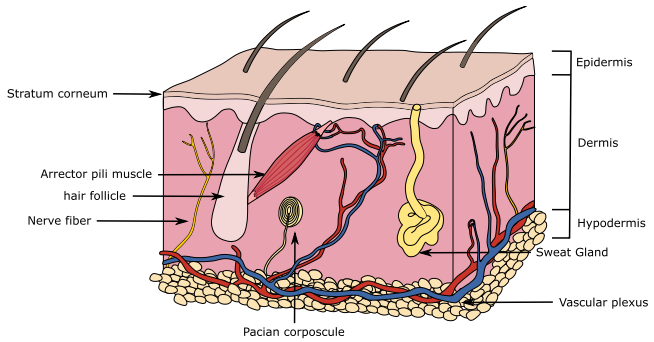

FIGURE 1. Anatomical structure of human skin.

curvature, interindividual differences) is analyzed. Section V discusses the first results obtained using micro-scale models. Finally, conclusions are drawn in Section VI.

II. FUNDAMENTALS OF MMW/BODY INTERACTIONS

The skin, covering about 95% of the human body, is the largest organ and is the main target tissue of mmWs. Its anatomical structure and main sub-structures are schematically represented in Fig. 1.

The skin is composed of two layers: epidermis and dermis. The epidermis contains the stratum corneum (SC), the uppermost layer composed of dead cells, and the viable epidermis beneath. The viable epidermis and dermis are usually considered as a single layer in the electromagnetic (EM) analysis as they have similar water concentration and thus similar EM properties at mmWs [14]. However, they are treated as two distinguished layers from the heat transfer viewpoint, as only dermis contains blood vessels. Note that dermis also includes micro structures (such as nerves, sebaceous glands, and pilosebaceous units) whose absorption may differ from the surrounding skin [15] (see Section V-A).

A. REFLECTION AND TRANSMISSION AT AIR/SKIN INTERFACE

Reflection and transmission at the air/skin interface depend on the dispersive EM properties of skin, as well as on the polarization and angle of incidence of the incident field. The skin permittivity has been directly measured or extrapolated to mmWs from microwave measurements in several studies reported in the literature and the main findings are summarized in [10], [11]. Variations of about 11% for the real part and 62% for the imaginary part are reported in [10] at 60 GHz depending on the tissue permittivity model. This results in variations of about 20% at 60 GHz in the power reflection coefficient for small angles of incidence [11]. For a normally impinging plane wave, in average 55% of the incident power is transmitted to the body at 30 GHz and 63% at 60 GHz [16]. Various physiological, environmental, and physical factors impact the magnitude of the transmission coefficient. For instance, the power transmission decreases to 53% (at 30 GHz) and 61% (at 60 GHz) for wet skin, as a consequence of an increase in the water content that results in a higher contrast at the air/skin interface. The impact of other factors, such as age, presence of clothing, local geometrical variation of the air/skin interface, EM source, and inter-individual variations is discussed in Section IV.

B. POWER ABSORPTION IN CUTANEOUS TISSUES

Due to a shallow penetration depth in the mmW range (e.g., roughly 0.85 mm at 30 GHz and 0.5 mm at 60 GHz for dry skin), only a small fraction of the penetrating to the body EM power is transmitted through skin and reaches the underlying fat layer (roughly 3% at 30 GHz and 0.3% at 60 GHz [17]). This demonstrates that subcutaneous fat and muscle almost do not impact the power absorption in the body above 30 GHz. The power absorbed in the skin depends on the SC thickness. For most body parts, SC thickness is in the 10–20 μm range, but it can reach 1.4 mm at some specific locations, such as palm and sole of the feet. It was demonstrated that, above 15 GHz, when the SC is thick (from 360 μm to 700 μm), it acts as a matching layer enhancing power transmission to the skin (above 60 GHz, the transmission coefficient can approach 100%) [18]. On the contrary, for a thin SC around 10–20 μm, no matching effect is observed.

C. MMW HEATING

Even if at mmWs almost all EM power is absorbed in the skin, the resulting heat spreads towards subcutaneous layers and reaches deeper tissues, including fat and muscle [18]. The skin thermal conductivity is equal to $\tau = 0.37\,\mathrm{W/(m^{\circ}C)}$, while the blood perfusion is in between the fat and the muscle ones and corresponds to $b_\mathrm{p} = 7440\,\mathrm{W/(m^3{}^{\circ}C)}$. Fat is a thermal insulator with a low thermal conductivity $\tau = 0.21\,\mathrm{W/(m^{\circ}C)}$ and blood perfusion $b_\mathrm{p} = 1900\,\mathrm{W/(m^3{}^{\circ}C)}$. The muscle tissue, with a higher $\tau = 0.49\,\mathrm{W/(m^{\circ}C)}$ and $b_\mathrm{p} = 2550\,\mathrm{W/(m^3{}^{\circ}C)}$, contributes strongly to heat dissipation [19].

For these reasons, using a homogenous skin model, the temperature elevation (ΔT) would be underestimated compared to a multilayer model. Note that, when adding only a fat layer with infinite extension to a finite-thickness skin layer, the temperature increase would be overestimated. The ΔT at steady state for a homogenous model is approximately half of the one obtained for a multi-layer model including fat and muscle for the same thermal exchange conditions at the air/skin interface at 30 GHz and 60 GHz [11], [18], [20].

D. DOSIMETRIC QUANTITIES AT MMWS

Two major international exposure guidelines and standards underwent a major revision in 2019 for International Electrical and Electronics Engineers (IEEE) Std. C95 [21] and in 2020 for the International Commission on Non-ionizing Radiation Protection (ICNIRP) guidelines [22]. One of the main modifications of the updated release concerns the dosimetric quantity above 6 GHz. The absorbed power density (S_ab)—referred as epithelial power density in IEEE Std. C95—is suggested as the main dosimetric quantity in the 6–300 GHz instead of the incident power density in the previous editions. Note that S_ab is an in-tissue metric and thus it accounts for

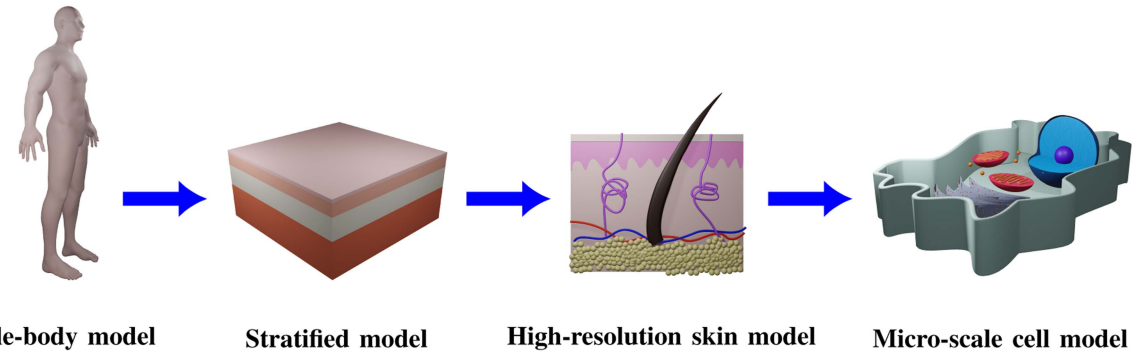

FIGURE 2. Example of models employed for exposure evaluation above 6 GHz: Full-body, mono-/multi-layer, anatomical skin, cell.

potential modifications of the exposure levels due the proximity of the body to the wireless device (such as standing wave between the body and wireless device or change in its radiation performance [23]).

The ICNIRP proposes two ways to calculate S_{ab}:

1) from the spatial distribution of specific absorption rate (SAR) in the near-surface tissue volume

$$S_{ab}^{(1)} = \frac{1}{A}\int\int_A dxdy \int_0^{Z_{max}} \rho(x,y,z)\cdot SAR(x,y,z)dz \quad (1)$$

2) from the electric and magnetic field at the skin surface

$$S_{ab}^{(2)} = \frac{1}{A}\int\int_A \mathrm{Re}\left[\boldsymbol{E}\times\boldsymbol{H}^*\right]\cdot d\boldsymbol{s}\,, \quad (2)$$

where $z = 0$ corresponds to the body surface, Z_{max} is the depth at which the EM power becomes negligibly small, A is the averaging area, ρ is the tissue density, $\boldsymbol{E}$ is the electric field, $\boldsymbol{H}$ is the magnetic field, $d\boldsymbol{s}$ is the integral variable vector normal to the surface, and the operators Re and $*$ denote the real part and complex conjugate, respectively.

To comply with the ICNIRP and IEEE limits, the absorbed power density averaged over a surface $A = 4$ cm^2 and a time interval of 6 min should not exceed 20 W/m^2 for general public and 100 W/m^2 for occupational exposure. Above 30 GHz, S_{ab} averaged over $A = 1$ cm^2 is restricted to twice the value allowed for $A = 4$ cm^2. For whole-body exposure, a further constraint is imposed on the averaged SAR that should not exceed 0.08 W/kg for general public and 0.4 W/kg for occupational exposure [22].

III. TISSUE EQUIVALENT MODELS AND PHANTOMS

Different models of various levels of complexity have been proposed to investigate physical mmW interactions with the human body (Fig. 2).

A. NUMERICAL MODELS

Anatomical 3D models of the human body have been developed from magnetic resonance imaging (MRI) data [24], [25] with a spatial resolution of at most 0.5 mm. While these models have been widely used for studies at the sub-6 GHz frequencies, their computational cost is extremely high at mmWs due to the increasing of the electrical size of the body with frequency and the fine spatial resolution required to comply with a shallow penetration depth (a 0.5-mm resolution is not sufficient to distinguish the different skin layers). For these reasons, the most commonly used tissue model for mmW dosimetry is a planar homogenous skin-equivalent model [26], locally representing a portion of the body. This simplified model reproduces the reflection coefficient from the human body and it is commonly used for dosimetry, on-body antenna characterization and body-centric propagation studies [12], [27].

In some studies, especially dealing with mmW-induced heating, the homogenous skin model may be replaced by a multi-layer model reproducing skin layers, subdermal fat and muscle [14], [18], [20], [28], [29], [30]. Indeed, as mentioned above, heat dissipation properties of dermis and epidermis are different and, in contrast to the mmWs field, the resulting heating reaches sub-contentious tissues. The main advantage of considering a planar mono- or multi-layer tissue model is the possibility to solve the problem in a closed form [31]. For a stratified n layer model with a normal impinging plane wave, the field distribution inside can be calculated as follows [32]:

$$\frac{\boldsymbol{E}_i(z_i)}{\boldsymbol{E}_0^+} = \frac{e^{jk_i(h_i-z_i)}\left(1+R_i e^{-j2k_i(h_i-z_i)}\right)}{\prod_{n=0}^{i-1}\frac{1}{1+r_n}e^{jk_{n+1}h_{n+1}}\left(1+r_nR_{n+1}e^{-j2k_{n+1}h_{n+1}}\right)} \quad (3a)$$

$$\frac{\boldsymbol{H}_i(z_i)}{\boldsymbol{H}_0^+} = \frac{\sqrt{\varepsilon_i}\,e^{jk_i(h_i-z_i)}\left(1-R_i e^{-j2k_i(h_i-z_i)}\right)}{\prod_{n=0}^{i-1}\frac{1}{1+r_n}e^{jk_{n+1}h_{n+1}}\left(1+r_nR_{n+1}e^{-j2k_{n+1}h_{n+1}}\right)}\,, \quad (3b)$$

where $R_i = E_i^-/E_i^+$ is the reflection coefficient at the i_{th} interface, k_i is the wave number in the i_{th} layer, and $r_i = (\sqrt{\varepsilon_i^*}-\sqrt{\varepsilon_{i+1}^*})/(\sqrt{\varepsilon_i^*}+\sqrt{\varepsilon_{i+1}^*})$, ε_i^* is the complex permittivity in the i_{th} layer. SAR can be calculated from the $\boldsymbol{E}$ field using a well-known relationship:

$$SAR_i = \frac{\sigma_i\left|E_{i_{rms}}\right|^2}{\rho_i}\,, \quad (4)$$

σ_i being the conductivity of the i-th layer. While SAR is not the primarily dosimetry quantity at mmWs, it is a useful

(a) (b)

FIGURE 3. Examples of (a) semi-solid [47] and (b) solid phantom [27].

intermediate metric for introducing a mmW heat source in the Bioheat transfer equation [33]

$$\rho_i c_i \frac{\partial T_i}{\partial t} = \nabla \cdot (\tau_i \nabla T) - b_p (T_i - T_{blood}) + Q_{m,i} + SAR_i \cdot \rho_i , \quad (5)$$

where c_i is the specific heat capacity, T_i is the tissue temperature, $Q_{m,i}$ is the heat generated by metabolism in the i-th layer, and T_{blood} is the blood temperature. In addition, S_{ab} can be calculated using (1) or (2) (with the knowledge of the $\boldsymbol{H}$ field).

Although planar models can be conveniently used for simplified analytical calculations, they no longer accurately represent realistic exposure scenarios when the body surface cannot be locally approximated as planar [34]. In this case, canonical curved [35], [36] or more complex anatomical (when the computational power allows for this) models [35], [37], [38], [39], [40], [41] can be used for numerical analysis.

The main limitation of homogenized macro-scale models is their disability to account for micro-scale effects. Indeed, biological tissues are neither homogeneous nor isotropic. Human skin is a heterogeneous structure hosting various sub-structures that are neglected in macro-dosimetry studies and may result in a local micro-scale absorption of the EM energy [15], [42] (Section V-A). This also applies to heterogeneous sub-cellular structures resulting in localized EM energy absorption inside biological cells [43] (Section V-B).

B. EXPERIMENTAL PHANTOMS

For measurements and validation of numerical results experimental phantoms are employed. As free water is the main constituent of soft biological tissues, including skin, semi-solid phantoms are commonly used for mmW dosimetry, on-body antenna characterization and propagation studies. In contrast to liquid phantoms commonly used below 6 GHz, they do not require a container. Several examples of semi-solid phantoms can be found in the literature at microwaves [44], [45]. In [46], the authors used gel materials to develop phantoms in the 2–26.5 GHz range with better mechanical and stability properties compared to agar- or gelatin-based phantoms. The first semi-solid phantom in the 60 GHz band was introduced in [47] (Fig. 3(a)). It contains de-ionized water, agar, polyethylene powder, TX-151, and sodium azide, and covers the 55–65 GHz range with ±10% accuracy in respect to the dry skin complex permittivity. A wide-band (20–100 GHz) semi-solid phantom was recently reported in [48]. The phantom, primarily made of water and glycerin, simulates the steady-state ΔT at the skin surface.

The main drawback of semi-solid phantoms is their limited lifetime due to water evaporation. To extend the lifetime, solid phantoms based on ceramic, graphite/carbon, and silicone rubber were proposed [49]. The difficulty of realizing a solid phantom at mmWs is the high loss tangent value (e.g., $\tan\delta = 1.37$ at 60 GHz), which is challenging to reproduce with standard materials and fabrication procedures. In [27], the authors suggested to reproduce the reflection coefficient at 60 GHz instead of the complex permittivity of the skin. The proposed phantom consists of a 1.3 mm-thick layer of silicone, charged with carbon powder and backed with a ground plane (Fig. 3(b)). By optimizing the silicone/carbon layer thickness the skin reflection coefficient can be reproduced for a wide range of the angles of incidence for both transverse electric (TE) and transverse magnetic (TM) polarizations. Recently, this concept of the reflectivity-based phantom design was adopted for dosimetry, enabling S_{ab} evaluation accounting for the antenna/body interaction [50], [51], [52].

IV. RECENT ADVANCEMENTS IN MACRO-SCALE MMW DOSIMETRY

This section provides an overview of recent studies dealing with the impact of exposure parameters on the mmW power absorption in the near-surface tissues.

A. ROLE OF ANGLE OF INCIDENCE, POLARIZATION, AND SOURCE TYPE

S_{ab} depends on the angle of incidence and polarization. The exposure to a normally-incident plane wave is compared to the case of oblique incidence for TE and TM polarizations in [53], [54]. When the angle of incidence (θ) increases, the transmission coefficient decreases monotonically for TE polarization. However, it increases for TM polarization till reaching its maximum value at the Brewster angle. Note that, even if the power transmission coefficient is higher at the Brewster

angle, S_{ab} is maximal for the normal incidence, resulting in the maximal heating at normal incidence.

It was demonstrated that a thick SC (20–700 μm) may act as a matching layer and the transmittance may be increased compared to the thin SC case (10–20 μm) [53]. Under unchanged exposure conditions, this results in an increase of S_{ab} compared to a thinner SC. At 30 GHz, the maximal transmittance—obtained for SC thicknesses acting as a matching layer—exceeds 80% from 0° to 20° for TE polarization and from 0° to 90° for TM polarization. At 60 GHz, it approaches 100% from 0° to 50° for both polarizations.

In [26], a 4 and a 8 element dipole arrays operating at 28 GHz are used to illuminate a planar homogenous skin model under near-field conditions. The study analyses the impact of the TE- and TM-like polarized waves, on the normal component (IPD_n) and the absolute value of the incident power density ($|IPD|$), as well as on the ΔT. The study reveals that IPD_n better correlates to the skin temperature rise independently of the angle of incidence (especially for $\theta < 30°$).

Finally, the effect of different antenna types (dipole, 4×4 dipole array, 4×4 patch array, slot array) for the normal incidence in the frequency range 10–90 GHz is investigated in [55]. The authors show that the ratio between the peak steady-state temperature rise and the peak spatial-average S_{ab} strongly depends on the antenna topology and the antenna-phantom separation (the maximum relative standard deviation among the considered antennas is 26.3% at 30 GHz for antenna-phantom distances > 5 mm).

B. DEPENDENCE ON AGE

Along with the massive development of 5G technologies, people of different age (from childhood to elderly age) are increasingly exposed to wireless devices due to the diversification of use cases.

The human body evolves with age, both in terms of EM properties (mainly due to age-dependent water concentration) and morphology. These changes impact the in-body mmW power absorption and the resulting temperature rise.

In [56], the exposure of 4 human models of the Virtual Population (Duke, Ella, Billie, and Thelonious) is investigated at 28 GHz. Three different scenarios are simulated: phone call, messaging, and browsing. A microstrip patch array is used as EM source and the problem is solved with the finite difference time domain (FDTD) method. The study does not find any noticeable difference in peak SAR and $S_{ab}^{(1)}$ between adults and children.

In [17], age-dependent variations of the skin thickness, permittivity, and blood flow are considered as parameters to study the EM power deposition and resulting heating at 26 GHz and 60 GHz.

The variations in tissue permittivity is obtained from Lichtenecker's exponential law [57],

$$\varepsilon^* = \varepsilon'_W{}^{\frac{\alpha-\alpha_A}{1-\alpha_A}} \varepsilon'_A{}^{\frac{1-\alpha}{1-\alpha_A}} \left(1 - j\frac{\varepsilon''_A}{\varepsilon'_A}\right). \quad (6)$$

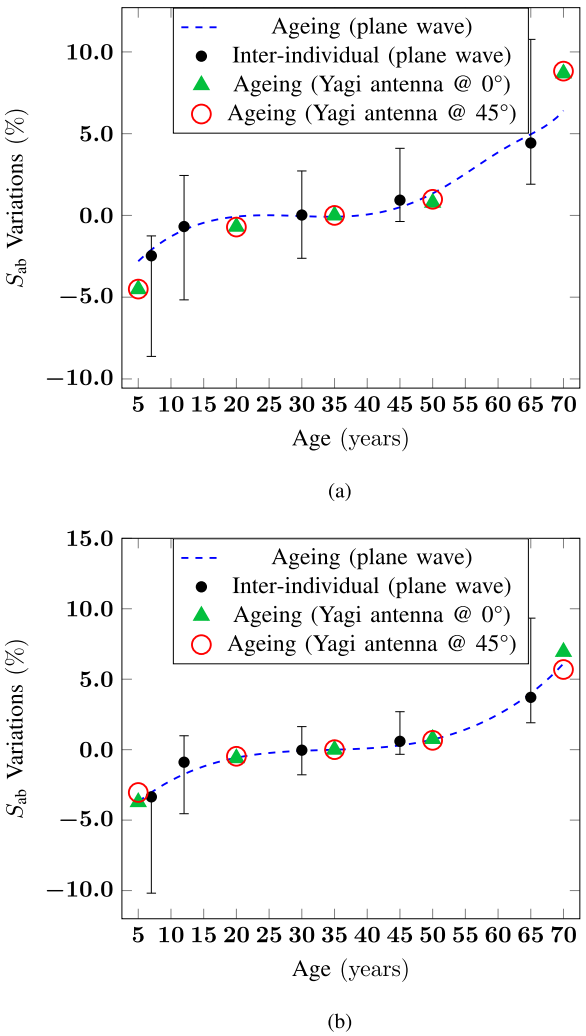

FIGURE 4. Variations of the S_{ab} averaged over a 4 cm^2 with respect to S_{ab} for a 35 years-old adult at (a) 26 GHz and (b) 60 GHz. The black bars refer to a Monte Carlo analysis with 10^6 trials considering the inter-individual variations in terms of the skin thickness and permittivity.

where the subscript A refers to the values for adults (35 years old), ε'_W is the real part of water permittivity [58], and $\alpha = TBW \cdot \rho$, being TBW the ratio of the amount of water in the human body and the person weight. With a normally impinging plane wave, the variations with age of the S_{ab} and peak SAR were found to be of 10% to 15% and are mainly due to permittivity change with age. Fig. 4 represents the variations of S_{ab} as a function of age with respect to the value for a 35 years old adult. The variations of steady-state heating with age follows the trend of S_{ab} and it increases over the lifespan of about 11% at 26 GHz and 13% at 60 GHz. Note that the skin blood flow responsible for cooling reduces with age [59], [60], [61], [62].

The results obtained for a plane-wave exposure are compared with the ones computed considering a Yagi-Uda antenna (4×1 array) as a source [16], [63] (Fig. 4). This is representative for 5G wireless devices, where the antennas are usually positioned at the edge of the device to reduce the body

shadowing and avoid the direct exposure of the user. In these conditions, $S_{ab}^{(2)}$ increases as a function of age with a plateau between 20 and 50 years. The plane-wave approximation slightly underestimates $S_{ab}^{(2)}$ at 26 GHz, while the variations with age at 60 GHz are almost identical for both excitations.

C. IMPACT OF CLOTHING

In some exposure scenarios, the exposed body area can be covered by a textile, in direct contact with the skin or separated from it by an air gap. For instance, this may occur when wearing a hat or using a tablet laying on the knees, but also in more specific conditions, such as the body scans at the airport.

The presence of a textile in contact or in proximity to the skin has a twofold effect: (i) from an EM point of view it modifies the propagation and may act as a matching layer; (ii) from a thermal viewpoint it reduces the heat exchange between the body and surrounding environment.

The effect of clothing on mmW absorption is analytically evaluated on a homogeneous skin model in [64] in the 30 GHz to 300 GHz range. The authors demonstrate that clothing can act as an impedance transformer enhancing absorption in the skin. For a textile with a permittivity of $4 - j0.1$, the peak in absorption may occur close to mmW wireless communication frequencies (e.g., at 32.9 GHz for a textile thickness of 1 mm and at 60.9 GHz for a textile thickness of 0.5 mm).

In [32], a four-layer tissue model composed of SC, viable epidermis and dermis, fat and muscle is used to analyze EM power absorption and resulting heating at 26 GHz and at 60 GHz. A layer of cotton ($\varepsilon_{cotton} = 2 - j0.04$ [65]) or wool ($\varepsilon_{wool} = 1.22 - j0.036$ [65]) is added on the top of the tissue model to simulate the presence of clothing, either in contact with skin or separated from it by an air gap. When illuminated by a normally impinging plane-wave, the presence of a textile in contact with skin can increase S_{ab} by up to 41.5% at 26 GHz and 34.4% at 60 GHz.

The maximal enhancement occurs for a textile thicknesses close to $(2n + 1)\lambda/4$, where n is an integer and λ is the wavelength inside the textile, confirming the findings of [64]. The presence of an air gap between a textile and skin can increase or decrease the absorption in the tissues depending on the textile permittivity and thicknesses of the air gap and textile. The heating is enhanced by the presence of a textile in contact with the skin compared to the bare skin (up to 52% at 26 GHz and 46% at 60 GHz). With an air gap between a textile and skin for the typical textile thicknesses (2 mm for wool and 0.2 mm for cotton), it ranges from −3.5% to 20.6% at 26 GHz and from −11.1% to 20.9% at 60 GHz. In [63], this study is extended to a directive multi-beam phased array of end-fire Yagi-Uda antennas. The results demonstrate that the plane-wave model overestimates S_{ab}.

In [66], the authors realize a Monte Carlo study to evaluate the impact of the textile material properties, incidence angle, and polarization on S_{ab} at 60 GHz. The considered textiles are cotton, wool, linen, leatherette, polyester fiber, and latex mattress. The authors employ a multilayer planar tissue model composed of epidermis, dermis, fat and muscle, with a textile layer on the top, separated by an air gap. This study showed that for TE and TM polarizations $S_{ab}^{(2)}$ decreases when the angle of the impinging plane wave increases. An oscillatory behavior of S_{ab} as a function of the gap thickness was noticed for angles of incidence $\leq 40^\circ$ independently of the polarization. For TM the dynamic range of the oscillations is in a stronger extent dependent on the material. The study confirms that (i) the worst-case scenario—corresponding to the highest exposure—occurs for normal incidence and that (ii) the presence an air gap between the textile and skin can decrease or increase EM absorption.

D. CURVED BODY PARTS

Planar body models can be used to assess local exposure of electrically large body parts, such as the torso. However, they may underestimate S_{ab} in the curved body parts, such as ears or hands. Indeed, for structures with the ratio between the curvature radius a and penetration depth δ below 5 (e.g., $a < 4.27$ mm at 30 GHz and $a < 2.39$ mm at 60 GHz), the decrease of the field inside the tissue cannot be considered as exponential anymore [34].

The effect of curvature on IPD has been recently investigated in [67], where IPD_n and $|IPD|$ are computed over a 9 cm radius sphere in presence of a dipole positioned at a distance 2 mm $\leq d \leq$ 150 mm from the surface. Above 30 GHz, when comparing $|IPD|$ averaged over the curved surface and a plane tangential to the sphere, the difference is lower than 1% independently of the distance. At 30 GHz, the highest relative difference between $|IPD|$ and IPD_n is up to 28.04% at $d = 2$ mm.

In [40], [41], the distribution of the electric field inside the near-surface tissues at 24 GHz for a planar multilayer slab is compared with the one obtained from anatomical 3D model of the wrist, the arm and the back showing a difference up to 2 dB. The effect of body curvature on the absorbed power and resulting heating in the 6–60 GHz range is also analyzed in [35]. The authors consider structures with a curvature radius $a = 2$–5 cm. They use a 2D cylindrical multilayer model composed of three layers (skin, fat, and muscle) and a 3D forearm model extracted from the XCAT phantom [68]. A plane wave is used as a source for the cylinder and an array of 4×1 half-wave dipole antennas for the 3D forearm model. The computed distributions are averaged by considering multiple definitions of the average volume and using the 2 equations of S_{ab} [(1) and (2)]. The study reveals that, depending on the definition of the volume used for the averaging, (2) may provide lower or higher S_{ab} than (1) and that the highest registered deviation between the two definitions is of about 15% at 6 GHz and below 3% above 20 GHz. When computing the heating factor (ratio of the surface temperature rise to the S_{ab}), for $a > 30$ mm and above 20 GHz, the results for 2D models agree well with those for planar models. In these conditions, only marginal differences exist when considering different definitions of the averaging volume used to compute S_{ab}^1. For the 3D model in presence of an array of dipoles, the heating factor generally decreases with the distance between

the antenna and the forearm. These heating factors are slightly higher than the ones computed for the 2D model with radii comparable to the forearm ones ($a = 30$ mm) [35].

In [36], the authors consider typical curvature radii of ears and fingers ($a = 1$–10 mm) exposed at 26 GHz and 60 GHz. In the EM analysis, the finger and ear are locally modelled with a 2D homogenous cylinder infinitely extended along its axis. In the thermal study, the same model is considered for the finger (a up to 10 mm). To model the ear ($1\text{ mm} \leq a \leq 5\text{ mm}$), the cylinder is extended by a parallelepiped to account for the heat exchange occurring between the tissues connecting ear to head. For the plane-wave excitation, S_{ab}^{max} remains lower than for a planar tissue model for TE polarization, while it is higher for TM polarization. The maximal differences are -38.2% and 72.3% at 26 GHz and -18.7% and 15% at 60 GHz. The resulting temperature rise is higher than that obtained for a planar model for both polarizations. For the ear, steady-state heating variations compared to a planar model are stronger than those of S_{ab}^{max} and reach 92.95% at 26 GHz and 103.62% at 60 GHz (TE polarization) and 93.11% at 26 GHz and 31.65% at 60 GHz (TM polarization).

The mmW exposure of human ears is further investigated in [37], [38]. In these studies, an anatomical model of an adult ear is illuminated by a plane wave at 26 GHz and 60 GHz. For a generic anatomical geometry the estimation of the averaged $S_{ab}^{(1)}$ and $S_{ab}^{(2)}$ is performed with a mesh-independent integration technique. Given the non-planarity of the surface, the averaging area used in (1) and (2) is not 1 cm^2 or 4 cm^2 but it is computed as the integral of the portion of the model surface enclosed by the projection of a 1 cm^2 or 4 cm^2 square. This resulting conformal area is typically bigger than that of the planar square. The analysis demonstrates that the maximal relative differences between the two definitions of S_{ab} with respect to the planar model value are up to 6.03% at 26 GHz and 4.34% at 60 GHz. Additionally, for all the considered scenarios and polarizations $S_{ab}^{(1)}$ was higher than $S_{ab}^{(2)}$.

E. INTER-INDIVIDUAL VARIABILITY

The dependence of the mmW power deposition and subsequent temperature rise on permittivity and thickness variations associated with the inter-individual differences is investigated in [28]. It is shown that the maximal relative standard deviation of ΔT is 8% and 7% above 30 GHz, when considering only thickness variations or combined thickness and permittivity variations, respectively. The decrease in the standard deviation associated to ΔT is attributed to the compensating effect of tissues thickness and permittivity variations when the heat rise is computed. The same authors repeated the analysis for multiple body areas (forearm, triceps, quadriceps, and abdomen) revealing that the results for the transmittance as a function of frequency are almost identical, while for ΔT the values for the abdomen are 8 to 12% higher than the ones in the forearm due to the thicker subdermal fat (3.89 ± 1.40 mm against 14.3 ± 7.5 mm).

V. RECENT ADVANCEMENTS IN MICRO-SCALE MMW DOSIMETRY

All the previously described studies considered the near-surface tissues as homogenous or layered, ignoring local micro-scale heterogeneity of the skin and human cells.

A. MICRO-SCALE ABSORPTION IN SKIN SUB-STRUCTURES

In [69], the effect of cutaneous blood vessels, hairs and sweat ducts is investigated at 42.25 GHz. The complex permittivity of these appendages differs from the ones of bulk human skin, thus impacting the local power absorption [69], [70]. The SAR induced inside the cutaneous blood vessels differs depending on the orientation of the incident field and exceeds by up to 40% the one in the surrounding dermis. Analysis of hair and sweat ducts revealed that the former is responsible for a greater distortion of the EM field than the latter. This may be explained by the contrast between the hair and skin permittivity, which is higher than the one between sweat gland and skin ($\varepsilon_{skin} = 12.7 - j16.6$, $\varepsilon_{sweat} = 15 - j27.1$, and $\varepsilon_{hair} = 2.6 - j0.1$ at 42.25 GHz).

Recently, the micro-scale power deposition in a complete set of human skin sub-structures at 60 GHz (including nerve fibers, blood vessels, lymphatic vessels, sebaceous glands, eccrine sweat glands, arrector pili muscle, hair, Meissner corpuscle, and Pacinian corpuscle) was investigated [15] (Fig. 5). The authors developed 3D models of these structures based on anatomical data and analyzed the electric field ($\boldsymbol{E}$) and power loss density ($PLD = SAR \cdot \rho$) considering a plane wave with different polarizations. Due to dielectric discontinuities between the skin appendages and surrounding dermis, the PLD increases at the interfaces, suggesting that the skin appendages may potentially be subject to higher local exposure. The maximum PLD (approximately 45% higher than surrounding skin) is observed in the eccrine sweat glands. The second and third highest PLD values are registered for the epidermal axons and the Pacinian corpuscle (37.9% and 32.5% higher than in the surrounding skin, respectively). The distribution of the PLD in a cutaneous nerve for TE and TM exposure is represented in Fig. 6.

In [42], the same group performed a thermal micro-dosimetry study showing that the maximal ΔT for a continous exposure to 10 W/m^2 occurs after 5 μs within the nerve and 10 μs in the capillary. The temperature is 19.2% (nerve) and 17.7% (capillary) higher than in the surrounding skin. The thermal equilibrium with skin was reached after about 10 ms. When considering pulses at the fluence limit suggested by ICNIRP (0.48 kJ/m^2) the peak temperature reached by nerves and capillaries was 34% and 24% higher than in the surrounding skin, respectively.

B. MICRO-SCALE POWER ABSORPTION AT SUB-CELLULAR LEVEL

The first study investigating micro-scale mmW absorption inside human cells is reported in [43]. A 2D keratinocyte model exposed at 60 GHz is studied using the finite element method (FEM) method. The generic cell model is designed based on

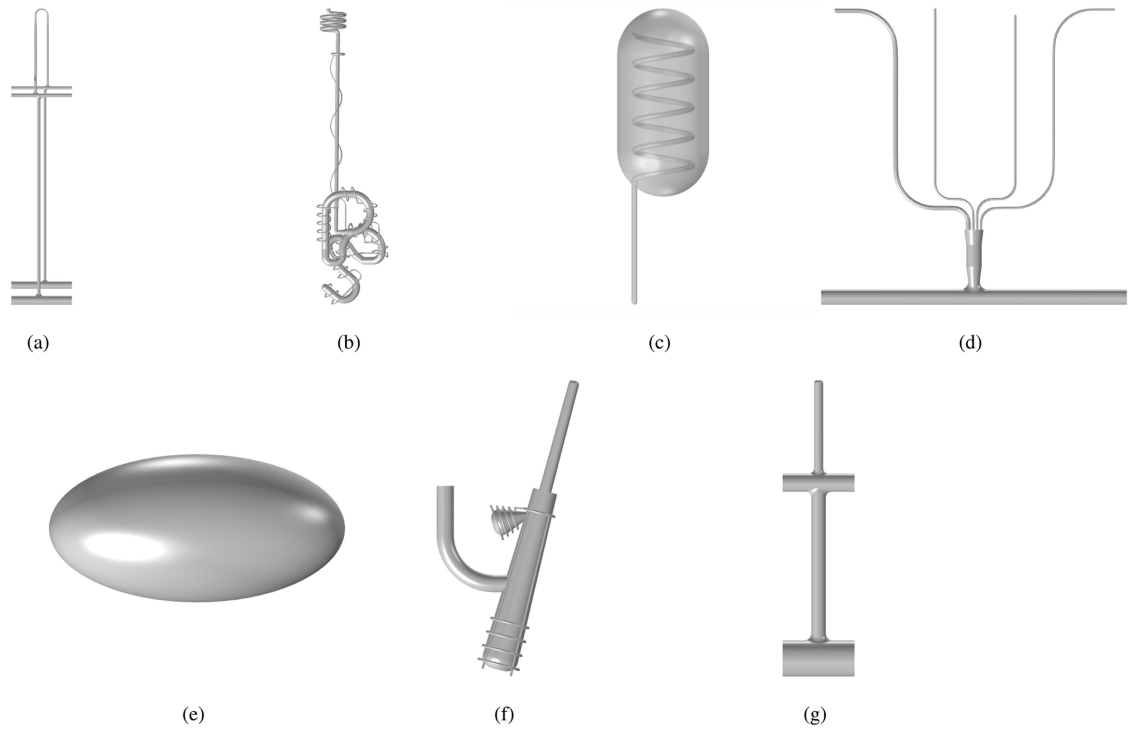

FIGURE 5. Numerical models of skin substructures: (a) Blood vessel, (b) eccrine sweat gland, (c) meissner corpuscle, (d) nerve fiber, (e) pacinian corpuscle, (f) pilosebaceous unit, and (g) lymphatic vessel.

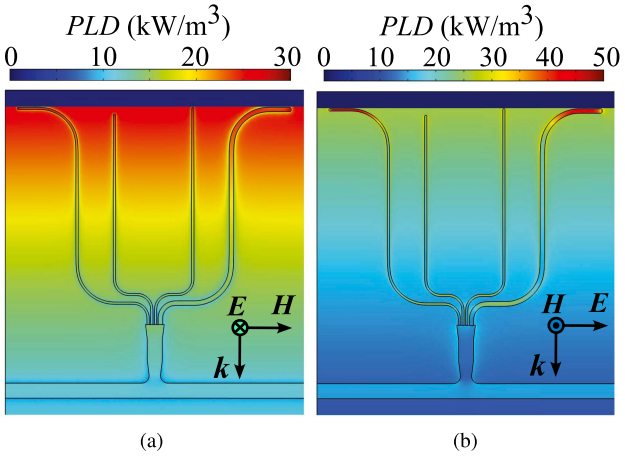

FIGURE 6. Distribution of the *PLD* in a cutaneous nerve for a normal impinging plane wave with (a) TE and (b) TM polarization.

electron microscopy images. It includes nucleus, endoplasmic reticulum, mitochondria, vesicles, and Golgi apparatus. The analysis reveals that 98.9% of the incident field penetrates the organelles at 60 GHz. The *PLD* averaged over the organelles' volume is in average 1.95% lower than that in the cytoplasm, while the averaged $\boldsymbol{E}$ in the nuclear pores is 1.1 times higher than the incident field and the averaged *PLD* in the same location was 1.2 times higher than in the cytoplasm. This suggests that, locally, the intracellular traffic is more exposed than the cytosol.

VI. CONCLUSION

This paper discusses the latest advancements in mmW dosimetry overviewing various physical aspects of mmW/body interactions at macro- and micro-scale.

Given the shallow penetration and the electrically large dimensions of the human body at these frequencies, whole body anatomical models have extremely high computational cost and insufficient spatial resolution. To decrease the computational cost, planar and curved mono- or multi-layer models have been used to analyze local exposure numerically or analytically. Micro-scale models reproducing skin and cell substructures have been recently introduced. Semi-solid and solid phantoms have been proposed to quantify the power deposition on the body surface and to investigate experimentally the antenna/body interactions at mmWs.

The effects of different parameters on the user exposure have been reported, including age, clothing, curvature of the body surface, characteristics of the impinging field, and inter-individual differences. The choice of the model used to simulate a given scenario is fundamental for an accurate evaluation of the EM exposure and the resulting temperature rise. Since at mmW frequencies the heat penetrates deeper in the body than the EM power, if the main focus of the analysis is the EM absorption, a monolayer skin model is sufficient. However, if the temperature is also of interest subjacent tissues should be included [14].

For what concerns the model parameters, when considering the permittivity values of the tissues, literature studies revealed that inter-individual differences or age impact the EM

power absorption and ΔT by approximatively 10–15% [17], [28]. Differences in thickness of different layers due to inter-individual differences or the on-body location are responsible of variations lower than 15%. The only exception is thick SC, that may increase the absorption up to 100% depending on the polarization of the impinging wave and angle of incidence.

It was demonstrated that, for all the scenarios that involve the presence of a clothing in contact with the skin, it is fundamental to account for the effect of textile. Indeed, for certain thicknesses, a textile layer in contact with the skin may act as a matching layer increasing the exposure level [32], [64]. The presence of an air gap between the textile and the skin produces fluctuations of S_{ab}, resulting in its increase or decrease depending on the textile and airgap thickness.

Several studies also demonstrated that, even if at mmWs the absorption is mainly superficial, the impact of the body curvature cannot be always neglected. Curved body structures may be subject to higher exposure, making planar models inaccurate to correctly evaluate the EM absorption and resulting heat rise of curved body parts [41]. For structures such as the ears, the variations of S_{ab} may be significant locally (up to roughly 20% at 60 GHz) and more limited when averaged spatially (of about 5% at 60 GHz) [71].

While all the models proposed to investigate the exposure at macro-level consider the human tissues as homogenous, recent micro-dosimetry studies demonstrated that the presence of substructures may modify locally the absorption and temperature distribution inside the tissues. As an example, *PLD* and temperature in the nerve axons can be up to 37.9% and 19.2% higher than in the surrounding skin, respectively. Note that the considered micro-scale model are generic and they do not take into account the dynamics and variability of biological cells. Stochastic studies are needed to get a deeper insight into these aspects. Furthermore, information regarding the effective EM properties of sub-cellular structures and their applicability at micro-scale is very limited. Progress in this direction would be an important step forward in definition of representative and computationally accurate micro-scale models.

REFERENCES

[1] W. Tang et al., "Wireless communications with reconfigurable intelligent surface: Path loss modeling and experimental measurement," *IEEE Trans. Wireless Commun.*, vol. 20, no. 1, pp. 421–439, Jan. 2021.

[2] Q. Qi, X. Chen, C. Zhong, and Z. Zhang, "Integrated sensing, computation and communication in B5G cellular Internet of Things," *IEEE Trans. Wireless Commun.*, vol. 20, no. 1, pp. 332–344, Jan. 2021.

[3] Federal Communications Commission (FCC), "Auction 102: Spectrum frontiers 24GHz." Accessed: Jun. 10, 2024. [Online]. Available: https://www.fcc.gov/auction/102

[4] Federal Communications Commission (FCC), "Auction 101: Spectrum frontiers 28GHz." Accessed: Jun. 10, 2024. [Online]. Available: https://www.fcc.gov/auction/101

[5] Federal Communications Commission (FCC), "Auction 103: Spectrum Frontiers Upper 37GHz, 39GHz, and 47GHz." Accessed: Jun. 10, 2024. [Online]. Available: https://www.fcc.gov/auction/103

[6] European Commission, "Shaping Europe's digital future." Accessed: Jun. 10, 2024. [Online]. Available: https://digital-strategy.ec.europa.eu/en/news/european-commission-harmonise-last-pioneer-frequency-band-needed-5g-deployment

[7] European Telecommunications Standards Institute (ETSI), "ETSI EN 302 567 V2.1.1 (201707)," 2017. Accessed: Jun. 10, 2024. [Online]. Available: https://www.etsi.org/deliver/etsi_en/302500_302599/302567/02.01.01_60/en_302567v020101p.pdf

[8] Federal Communications Commission (FCC), "Fact sheet on spectrum frontiers item." Accessed: Jun. 10, 2024. [Online]. Available: https://www.fcc.gov/document/fact-sheet-spectrum-frontiers-item

[9] Apple, "5G and LTE, Find the iPhone that's right for your country or region." Accessed: Jun. 10, 2024. [Online]. Available: https://www.apple.com/iphone/cellular/

[10] M. Zhadobov, N. Chahat, R. Sauleau, C. L. Quement, and Y. L. Drean, "Millimeter-wave interactions with the human body: State of knowledge and recent advances," *Int. J. Microw. Wireless Technol.*, vol. 3, no. 2, pp. 237–247, Apr. 2011.

[11] T. Wu, T. S. Rappaport, and C. M. Collins, "Safe for generations to come: Considerations of safety for millimeter waves in wireless communications," *IEEE Microw. Mag.*, vol. 16, no. 2, pp. 65–84, Mar. 2015.

[12] M. Zhadobov, C. Leduc, A. Guraliuc, N. Chahat, and R. Sauleau, "Antenna/human body interactions in the 60GHz band: State of knowledge and recent advances," in *Advances in Body-Centric Wireless Communication: Applications and State-of-the-Art*, Eds. Stevenage, U.K.: Institution of Engineering and Technology, 2016, pp. 97–142.

[13] A. Hirata et al., "Human exposure to radiofrequency energy above 6GHz: Review of computational dosimetry studies," *Phys. Med. Biol.*, vol. 66, no. 8, Apr. 2021, Art. no. 08TR01.

[14] M. C. Ziskin, S. I. Alekseev, K. R. Foster, and Q. Balzano, "Tissue models for RF exposure evaluation at frequencies above 6GHz," *Bioelectromagnetics*, vol. 39, no. 3, pp. 173–189, Apr. 2018.

[15] Z. Haider, Y. L. Drean, G. Sacco, D. Nikolayev, R. Sauleau, and M. Zhadobov, "High-resolution model of human skin appendages for electromagnetic dosimetry at millimeter waves," *IEEE J. Microwaves*, vol. 2, no. 1, pp. 214–227, Jan. 2022.

[16] G. Sacco, D. Nikolavev, R. Sauleau, and M. Zhadobov, "Age dependence of human exposure in emerging 5G bands: Comparison between plane-wave exposure and multi-beam antennas," in *Proc. IEEE 34th Gen. Assem. Sci. Symp. Int. Union Radio Sci.*, 2021, pp. 1–4.

[17] G. Sacco, S. Pisa, and M. Zhadobov, "Age-dependence of electromagnetic power and heat deposition in near-surface tissues in emerging 5G bands," *Sci. Rep.*, vol. 11, no. 1, Feb. 2021, Art. no. 3983.

[18] A. Christ, T. Samaras, E. Neufeld, and N. Kuster, "RF-induced temperature increase in a stratified model of the skin for plane-wave exposure at 6-100GHz," *Radiat. Protection Dosimetry*, vol. 188, no. 3, pp. 350–360, Jun. 2020.

[19] P. A. Hasgall et al., "IT'IS database for thermal and electromagnetic parameters of biological tissues version 4.0," May 2018. [Online]. Available: https://www.itis.swiss/virtual-population/tissue-properties/overview/

[20] A. Kanezaki, A. Hirata, S. Watanabe, and H. Shirai, "Parameter variation effects on temperature elevation in a steady-state, one-dimensional thermal model for millimeter wave exposure of one- and three-layer human tissue," *Phys. Med. Biol.*, vol. 55, no. 16, pp. 4647–4659, Aug. 2010.

[21] *IEEE Standard for Safety Levels With Respect to Human Exposure to Electric, Magnetic, and Electromagnetic Fields, 0Hz to 300GHz*, Standard IEEE C95. 1-2019, Nov. 2019.

[22] International Commission on Non-Ionizing Radiation Protection (ICNIRP), "Guidelines for limiting exposure to electromagnetic fields (100kHz to 300GHz)," *Health Phys.*, vol. 118, no. 5, pp. 483–524, May 2020.

[23] M. Ziane, R. Sauleau, and M. Zhadobov, "Antenna/body coupling in the near-field at 60GHz: Impact on the absorbed power density," *Appl. Sci.*, vol. 10, no. 21, Oct. 2020, Art. no. 7392.

[24] T. Nagaoka et al., "Development of realistic high-resolution whole-body voxel models of Japanese adult males and females of average height and weight, and application of models to radio-frequency electromagnetic-field dosimetry," *Phys. Med. Biol.*, vol. 49, no. 1, pp. 1–15, Jan. 2004.

[25] M.-C. Gosselin et al., "Development of a new generation of high-resolution anatomical models for medical device evaluation: The virtual population 3.0," *Phys. Med. Biol.*, vol. 59, no. 18, pp. 5287–5303, Sep. 2014.

[26] T. Nakae, D. Funahashi, J. Higashiyama, T. Onishi, and A. Hirata, "Skin temperature elevation for incident power densities from dipole arrays at 28GHz," *IEEE Access*, vol. 8, pp. 26863–26871, 2020.

[27] A. R. Guraliuc, M. Zhadobov, O. D. Sagazan, and R. Sauleau, "Solid phantom for body-centric propagation measurements at 60GHz," *IEEE Trans. Microw. Theory Techn.*, vol. 62, no. 6, pp. 1373–1380, Jun. 2014.

[28] K. Sasaki, M. Mizuno, K. Wake, and S. Watanabe, "Monte Carlo simulations of skin exposure to electromagnetic field from 10GHz to 1 THz," *Phys. Med. Biol.*, vol. 62, no. 17, pp. 6993–7010, Aug. 2017.

[29] A. Kanezaki, S. Watanabe, A. Hirata, and H. Shirai, "Theoretical analysis for temperature elevation of human body due to millimeter wave exposure," in *Proc. IEEE Cairo Int. Biomed. Eng. Conf.*, 2008, pp. 1–4.

[30] A. Kanezaki, A. Hirata, S. Watanabe, and H. Shirai, "Effects of dielectric permittivities on skin heating due to millimeter wave exposure," *BioMedical Eng. OnLine*, vol. 8, no. 1, 2009, Art. no. 20.

[31] S. Alekseev and M. Ziskin, "Human skin permittivity determined by millimeter wave reflection measurements," *Bioelectromagnetics*, vol. 28, no. 5, pp. 331–339, Jul. 2007.

[32] G. Sacco, S. Pisa, and M. Zhadobov, "Impact of textile on electromagnetic power and heating in near-surface tissues at 26GHz and 60GHz," *IEEE J. Electromagn., RF, Microw. Med. Biol.*, vol. 5, no. 3, pp. 262–268, Dec. 2020.

[33] H. H. Pennes, "Analysis of tissue and arterid blood temperatures in the resting human forearm," *J. Appl. Physiol.*, vol. 1, no. 2, pp. 93–122, Aug. 1948.

[34] F. S. Barnes and B. Greenebaum, "Handbook of biological effects of electromagnetic fields," 3rd ed., Boca Raton, US: CRC Press/Taylor & Francis Group, 2006.

[35] Y. Diao, E. A. Rashed, and A. Hirata, "Assessment of absorbed power density and temperature rise for nonplanar body model under electromagnetic exposure above 6GHz," *Phys. Med. Biol.*, vol. 65, no. 22, Nov. 2020, Art. no. 224001.

[36] G. Sacco, Z. Haider, and M. Zhadobov, "Exposure levels induced in curved body parts at mmWaves," *IEEE J. Electromagn., RF, Microw. Med. Biol.*, vol. 6, no. 3, pp. 413–419, Sep. 2022.

[37] A. L. Kapetanovic, G. Sacco, D. Poljak, and M. Zhadobov, "Assessment of area-average absorbed power density on realistic tissue models at mmWaves," in *Proc. IEEE MTT-S Int. Microw. Biomed. Conf.*, 2022, pp. 153–155.

[38] A. L. Kapetanovic, G. Sacco, D. Poljak, and M. Zhadobov, "Area-averaged transmitted and absorbed power density on a realistic ear model," *IEEE J. Electromagn., RF, Microw. Med. Biol.*, vol. 7, no. 1, pp. 39–45, Mar. 2023.

[39] A. R. Guraliuc, M. Zhadobov, R. Sauleau, L. Marnat, and L. Dussopt, "Near-field user exposure in forthcoming 5G scenarios in the 60GHz band," *IEEE Trans. Antennas Propag.*, vol. 65, no. 12, pp. 6606–6615, Dec. 2017.

[40] M. Colella, S. D. Meo, M. Liberti, M. Pasian, and F. Apollonio, "Numerical comparison of plane wave propagation inside realistic anatomical models and multilayer slabs," in *Proc. IEEE 52nd Eur. Microw. Conf.*, 2022, pp. 800–803.

[41] M. Colella, S. D. Meo, M. Liberti, M. Pasian, and F. Apollonio, "Advantages and disadvantages of computational dosimetry strategies in the low mmW range: Comparison between multilayer slab and anthropomorphic models," *IEEE Trans. Microw. Theory Techn.*, vol. 71, no. 10, pp. 4533–4545, Oct. 2023.

[42] Z. Haider, J. Modolo, M. Liberti, F. Apollonio, and M. Zhadobov, "Millimeter-wave induced heating of cutaneous nerves and capillaries," *IEEE J. Microwaves*, vol. 3, no. 1, pp. 170–180, Jan. 2023.

[43] Z. Haider et al., "Local dosimetry at cellular and subcellular level in HF and millimeter-wave bands," *IEEE J. Microwaves*, vol. 1, no. 4, pp. 1003–1014, Oct. 2021.

[44] K. Ito, K. Furuya, Y. Okano, and L. Hamada, "Development and characteristics of a biological tissue-equivalent phantom for microwaves," *Electron. Commun. Jpn. (Part I, Commun.)*, vol. 84, no. 4, pp. 67–77, Apr. 2001.

[45] T. Takimoto, T. Onishi, K. Saito, M. Takahashi, S. Uebayashi, and K. Ito, "Characteristics of biological tissue equivalent phantoms applied to UWB communications," *Electron. Commun. Jpn. (Part I, Commun.)*, vol. 90, no. 5, pp. 48–55, May 2007.

[46] S. Castello-Palacios, C. Garcia-Pardo, M. Alloza-Pascual, A. Fornes-Leal, N. Cardona, and A. Valles-Lluch, "Gel phantoms for body microwave propagation in the (2 to 26.5) GHz frequency band," *IEEE Trans. Antennas Propag.*, vol. 67, no. 10, pp. 6564–6573, Oct. 2019.

[47] N. Chahat, M. Zhadobov, and R. Sauleau, "Broadband tissue-equivalent phantom for BAN applications at millimeter waves," *IEEE Trans. Microw. Theory Techn.*, vol. 60, no. 7, pp. 2259–2266, Jul. 2012.

[48] K. Sasaki et al., "Design of a skin equivalent phantom for estimating surface temperature elevation due to human exposure to electromagnetic fields from 10 to 100GHz," *IEEE Trans. Electromagn. Compat.*, vol. 63, no. 5, pp. 1631–1639, Oct. 2021.

[49] Speag. Accessed: Jun. 10, 2024. [Online]. Available: https://speag.swiss/products/em-phantoms/overview-2/

[50] M. Ziane, M. Zhadobov, and R. Sauleau, "High-resolution technique for near-field power density measurement accounting for antenna/body coupling at millimeter waves," *IEEE Antennas Wireless Propag. Lett.*, vol. 20, no. 11, pp. 2151–2155, Nov. 2021.

[51] M. Ziane, A. Boriskin, and M. Zhadobov, "Near-field power density mapping of close-to-body low-power mmWave devices," *IEEE Antennas Wireless Propag. Lett.*, vol. 22, no. 10, pp. 2347–2351, Oct. 2023.

[52] M. Ziane, A. Boriskin, C. Leconte, L. L. Coq, and M. Zhadobov, "Novel technique for in-body absorbed power density assessment based on free-space e-field measurement," *IEEE Trans. Microw. Theory Techn.*, early access, Dec. 5, 2023.

[53] T. Samaras and N. Kuster, "Theoretical evaluation of the power transmitted to the body as a function of angle of incidence and polarization at frequencies GHz and its relevance for standardization: Enhanced power transmittance above 6GHz," *Bioelectromagnetics*, vol. 40, no. 2, pp. 136–139, Feb. 2019.

[54] K. Li, K. Sasaki, S. Watanabe, and H. Shirai, "Relationship between power density and surface temperature elevation for human skin exposure to electromagnetic waves with oblique incidence angle from 6GHz to 1 THz," *Phys. Med. Biol.*, vol. 64, no. 6, Mar. 2019, Art. no. 065016.

[55] K. Li et al., "Intercomparison of calculated incident power density and temperature rise for exposure from different antennas at 10–90GHz," *IEEE Access*, vol. 9, pp. 151654–1516663, 2021.

[56] M. S. Morelli, S. Gallucci, B. Siervo, and V. Hartwig, "Numerical analysis of electromagnetic field exposure from 5G mobile communications at 28GHz in adults and children users for real-world exposure scenarios," *Int. J. Environ. Res. Public Health*, vol. 18, no. 3, Jan. 2021, Art. no. 1073.

[57] J. Wang, O. Fujiwara, and S. Watanabe, "Approximation of aging effect on dielectric tissue properties for SAR assessment of mobile telephones," *IEEE Trans. Electromagn. Compat.*, vol. 48, no. 2, pp. 408–413, May 2006.

[58] W. J. Ellison, "Permittivity of pure water, at standard atmospheric pressure, over the frequency range 0–25THz and the temperature range 0–100 °C," *J. Phys. Chem. Reference Data*, vol. 36, no. 1, pp. 1–18, Mar. 2007.

[59] G. A. Rooke, M. V. Savage, and G. L. Brengelmann, "Maximal skin blood flow is decreased in elderly men," *J. Appl. Physiol.*, vol. 77, no. 1, pp. 11–14, Jul. 1994.

[60] K. B. Stansberry, M. A. Hill, S. A. Shapiro, P. M. McNitt, B. A. Bhatt, and A. I. Vinik, "Impairment of peripheral blood flow responses in diabetes resembles an enhanced aging effect," *Diabetes Care*, vol. 20, no. 11, pp. 1711–1716, Nov. 1997.

[61] Y. Tsuchida, "The effect of aging and arteriosclerosis on human skin blood flow," *J. Dermatological Sci.*, vol. 5, no. 3, pp. 175–181, Jun. 1993.

[62] D. N. Proctor, K. U. Le, and S. J. Ridout, "Age and regional specificity of peak limb vascular conductance in men," *J. Appl. Physiol.*, vol. 98, no. 1, pp. 193–202, Jan. 2005.

[63] G. Sacco, D. Nikolayev, R. Sauleau, and M. Zhadobov, "Antenna/human body coupling in 5G millimeter-wave bands: Do age and clothing matter?," *IEEE J. Microwaves*, vol. 1, no. 2, pp. 593–600, Apr. 2021.

[64] O. Gandhi and A. Riazi, "Absorption of millimeter waves by human beings and its biological implications," *IEEE Trans. Microw. Theory Techn.*, vol. 34, no. 2, pp. 228–235, Feb. 1986.

[65] A. R. Guraliuc, M. Zhadobov, G. Valerio, N. Chahat, and R. Sauleau, "Effect of textile on the propagation along the body at 60GHz," *IEEE Trans. Antennas Propag.*, vol. 62, no. 3, pp. 1489–1494, Mar. 2014.

[66] K. Li, "Monte Carlo simulation of clothed skin exposure to electromagnetic field with oblique incidence angles at 60GHz," *Front. Public Health*, vol. 10, 2022, Art. no. 795414.

[67] A. L. Kapetanovic and D. Poljak, "Assessment of incident power density on spherical head model up to 100GHz," *IEEE Trans. Electromagn. Compat.*, vol. 64, no. 5, pp. 1296–1303, Oct. 2022.
[68] W. P. Segars, G. Sturgeon, S. Mendonca, J. Grimes, and B. M. W. Tsui, "4D XCAT phantom for multimodality imaging research: 4D XCAT phantom for multimodality imaging research," *Med. Phys.*, vol. 37, no. 9, pp. 4902–4915, Aug. 2010.
[69] S. I. Alekseev and M. C. Ziskin, "Millimeter-wave absorption by cutaneous blood vessels: A computational study," *IEEE Trans. Biomed. Eng.*, vol. 56, no. 10, pp. 2380–2388, Oct. 2009.
[70] S. Alekseev and M. Ziskin, "Distortion of millimeter-wave absorption in biological media due to presence of thermocouples and other objects," *IEEE Trans. Biomed. Eng.*, vol. 48, no. 9, pp. 1013–1019, Sep. 2001.
[71] A. L. Kapetanovic, G. Sacco, D. Poljak, and M. Zhadobov, "Area-averaged transmitted and absorbed power density on a realistic ear model," *IEEE J. Electromagn., RF, Microw. Med. Biol.*, vol. 7, no. 1, pp. 39–45, Mar. 2023.

GIULIA SACCO (Member, IEEE) received the M.S. (summa cum laude) degree in biomedical engineering and the Ph.D. (cum laude and with the Doctor Europaeus label) degree in information and communication technology from the Sapienza University of Rome, Rome, Italy, in 2017 and 2021, respectively. She was a Visiting Researcher with Stiching imec Eindhoven, Eindhoven, The Netherlands, from April 2019 to September 2019. She is currently a Research Fellow with Institut d'Électronique et des Technologies du numérique, Rennes, France. Her scientific and research interests include the field of innovative biomedical applications of electromagnetic fields and radars for vital signs monitoring. Dr. Sacco was the recipient of the Best Student Paper Award at Photonics & Electromagnetics Research Symposium (PIERS) 2019 and Best Student Paper Award at the 33rd General Assembly and Scientific Symposium (GASS) of the International Union of Radio Science (Union Radio Scientifique Internationale-URSI) 2020.

MAXIM ZHADOBOV (Senior Member, IEEE) received the Ph.D. and Habilitation à Diriger des Recherches degrees from the Institut d'Electronique et des Technologies du numerique (IETR), University of Rennes 1, Rennes, France, in 2006 and 2016, respectively. He was a Postdoctoral Researcher with the Center for Biomedical Physics, Temple University, Philadelphia, PA, USA, until 2008, and then joined the French National Center for Scientific Research (CNRS), Paris, France. He is currently a Senior Research Scientist with the IETR/CNRS in charge of the Electromagnetic Waves in Complex Media (eWAVES) research group. He has coauthored five book chapters, 90 research papers in peer-reviewed international journals, and more than 200 contributions to conferences and workshops. His research interests include innovative biomedical applications of electromagnetic fields and associated technologies. His review article in the *International Journal of Microwave and Wireless Technologies* was the most cited paper in 2016–2023. A paper published by his research group in 2019 is in journal Top 100 of *Nature Scientific Reports*. He has been involved in 26 research projects (15 as PI). Dr. Zhadobov was the TPC Co-Chair of BioEM 2021/2020. He was a TPC member and/or session organizer at international conferences, including IEEE AP-S/URSI 2024, URSI AT-RASC 2024, AES 2023, BioEM 2023, EUMW2022, IEEE IMBioC 2022, AT-AP-RASC 2022, BioEM 2019, EuMW 2019, IEEE iWEM 2017, MobiHealth 2015–2017, BodyNets 2016, and IMWS-Bio 2014. He was an elected member of EBEA Council from 2017 to 2021. He is a member of IEEE TC95.4 and President of URSI France Commission K. He is an Associate Editor for IEEE JOURNAL OF ELECTROMAGNETICS, RF AND MICROWAVES IN MEDICINE AND BIOLOGY and was the Guest Editor of several special issues, including Human Exposure in 5G and 6G Scenarios of Applied Sciences and Advanced Electromagnetic Biosensors for Medical, Environmental and Industrial Applications of Sensors. He was also on review boards of more than 15 international journals and conferences, and has been acting as an expert at research councils worldwide. He was the recipient of the Research & Innovation Award of Grand Ouest Foundation in 2022, CNRS Medal in 2018, EBEA Award for Excellence in Bioelectromagnetics in 2015, and Brittany's Young Scientist Award in 2010. Since 2010, the Ph.D. students he worked with received seven national scientific awards and six awards from the Bioelectromagnetics Society, URSI, IEEE Antennas and Propagation and IEEE Microwave Theory and Technology Societies.